

Quantitative Evaluation of Base and Detail Decomposition Filters Based on their Artifacts

Charles Hessel and Jean-Michel Morel

Abstract—This paper introduces a quantitative evaluation of filters that seek to separate an image into its large-scale variations, the base layer, and its fine-scale variations, the detail layer. Such methods have proliferated with the development of HDR imaging and the proposition of many new tone-mapping operators. We argue that an objective quality measurement for all methods can be based on their artifacts. To this aim, the four main recurrent artifacts are described and mathematically characterized. Among them two are classic, the luminance halo and the staircase effect, but we show the relevance of two more, the contrast halo and the compartmentalization effect. For each of these artifacts we design a test-pattern and its attached measurement formula. Then we fuse these measurements into a single quality mark, and obtain in that way a ranking method valid for all filters performing a base+detail decomposition. This synthetic ranking is applied to seven filters representative of the literature and shown to agree with expert artifact rejection criteria.

Index Terms—objective image quality assessment, artifact measurement, base and detail decomposition, edge-aware smoothing filters.

Supplementary Material—Supplementary material for this paper can be found [here](#)¹.

I. INTRODUCTION

This paper studies image-processing filters that seek to separate an image into its large-scale variations, the base layer, and its fine-scale variations, the detail layer. Such methods are also referred to as edge-aware smoothing filters or cartoon+texture decomposition. A base+detail decomposition is the core of photo editing tools such as high-dynamic range tone mapping and local contrast enhancement. These algorithms aim at adding more clarity to the image by enhancing its detail.

A key requirement of such algorithms is the absence of artifacts, that originate from wrong attribution of some base part to the detail. In the context of contrast enhancement, in which the dynamic of the base is reduced and the detail dynamics increased, minor errors may result in conspicuous and unacceptable artifacts. We illustrate four of them in Figure 1. Motivated by the rapid development of digital photography, many decomposition filters have been proposed since the early 2000s. The presence of artifacts is acknowledged in most of them. It often serves as argument for their comparison, but such arguments have so far remained partial and merely qualitative.

This study intends to provide experts with a clear identification of the different types of artifacts in the base and detail

decomposition filters together with a methodology to measure each of them and to eventually give a reliable mark to each method. To that aim, we shall first perform an analysis of the most prominent base+detail decomposition filters and proceed to the identification of their respective artifacts. We then propose specific patterns, designed to stir each targeted artifact. Our mathematical definition of each artifact, coupled with its dedicated pattern, yields a measure that can be associated with each edge-aware smoothing filter. We are led to address the delicate problem of comparing fairly the filters based on pattern measurements. This requires a cross-calibration of base+detail filters so that they yield the same amount of detail. Once the parameters of the filters have been fixed accordingly, they can be applied to our patterns and yield a mark for each filter and each artifact. The last problem addressed here is to find the adequate weights for each artifact measurement, taking into account that some of them like the luminance halo are less annoying than for example the staircase effect. To find the right combination, we rely on annotations by experts. In that way we transform partial and subjective rejections by experts into an automatic global quality measurement for each filter. It delivers a rank for any base+detail method and actually leads us to rank objectively the state of the art methods.

In summary, we make the following contributions:

- We draw up a list of artifacts likely to appear in any base and detail decomposition filter;
- We analyze and explain the identified artifacts, and propose for each of them a pattern-measure pair to quantitatively evaluate its presence in any filter;
- We design a simple cross-calibration method to set the filters' parameters, so that they can be compared fairly;
- We involve an expert evaluation (rather than non-specialist subjects) to fuse the independent measures of artifacts into a single meaningful score;
- We rank representative classic filters according to our measures, thus clarifying what filters are best suited for contrast enhancement.

The paper is organized as follows:

- We first discuss in Section II the broader topic of image quality assessment, that has related methodological issues, and the existing descriptions and measures of certain artifacts;
- Section III reviews seven classic filters, each being arguably the most representative filter in a different class of filters performing base+detail decomposition. We analyze the guided filter, the weighted least squares filter, the local Laplacian filters, the total variation with L^1 data fidelity, the image smoothing via L^0 gradient minimization filter,

Charles Hessel and Jean-Michel Morel are with CMLA, ENS Cachan, CNRS, Université Paris-Saclay, 94235 Cachan, France

¹<http://dev.ipol.im/~hessel/publications/quantitativeArtifactEvaluation/SupplementaryMaterial.pdf>

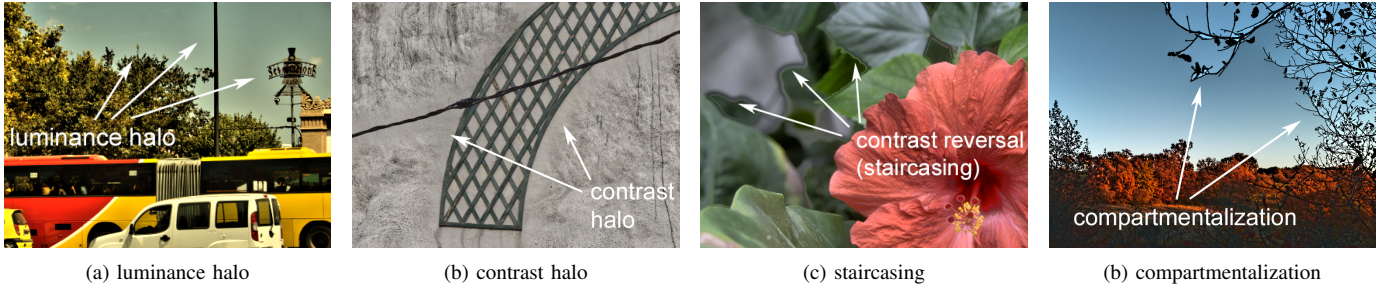


Figure 1. A panorama of the image enhancement artifacts. In those contrast-enhanced images, the detail layer is amplified by $enhance(u) = \frac{1-\beta}{2}D + \beta \times base(u) + \alpha \times detail(u)$. In this formula, D is the input dynamic range, $\beta = .75$ and $\alpha = 3$ (except for the contrast halo where we used $\alpha = 6$). The luminance halo is the most classic and well known artifact. The contrast halo attenuates texture near edges. The staircasing creates bands with inverted contrast often called the “contrast reversal” artifact. Compartmentalization effect breaks the unity of homogeneous regions.

and the domain transform.

- We define the artifacts in Section IV, give their mathematical definition and design patterns to measure them.
- Section V addresses the cross-calibration of filters previous to their ranking.
- Section VI performs the ranking and matches it to expert evaluations.

II. RELATED WORK

Enhancement filters such as tone-mapping operators and local contrast enhancement filters are prone to artifacts. Indeed, the detail layer’s dynamic is expanded, thus enhancing any error in the base+detail decomposition, that becomes a conspicuous artifact. To the best of our knowledge, no previous paper has proposed ranking filters by measuring their artifacts. In the Reinhard *et al.* book on high dynamic range imaging [1], one can read for example that

Recently, some attempts of no-reference image contrast, sharpness, color saturation, and presence of noise evaluation have been reported; however, combining all these factors into a meaningful quality prediction is a difficult problem.

Numerous perceptual studies have been carried out for high dynamic range (HDR) imaging, to evaluate the subjective quality of images obtained by different tone-mapping operators (TMOs). As stated by Drago *et al.* [2]:

Essentially, tone mapping should provide drastic contrast reduction from scene values to displayable ranges while preserving the image details essential to appreciate the scene content.

Eilertsen *et al.* [3] classify the TMOs in three categories: the *visual system simulators* (VSS) that simulate the human visual system, the *scene reproduction* (SRP) operators that try to reproduce as faithfully as possible the HDR scene, and the *best subjective quality* (BSQ) operators that are designed to produce good-looking images irrespective of the original content. Technically, one can distinguish two types of TMOs: the *global* and the *local* operators. The global operators apply the same correction to pixels with the same color, whereas in the local operators the correction depends on the local content. Global TMOs are faster and generate fewer artifacts, but local TMOs better preserve the local contrast. A base+detail decomposition therefore is the core of most local TMOs [4].

A first set of studies assesses image quality based on evaluations by non-expert subjects. This concerns most of the published evaluation methods, which then can be divided in two categories. The first category measures the similarity of a tone-mapped image to the original HDR scene or to the HDR image displayed with an adapted screen [5]–[9]. The second set of studies propose subjective image quality evaluation without referring it to the original one [3], [7], [8], [10]–[14].

Another group of papers proposes objective measurements for basic properties of tone-mapped images, such as color, contrast and well-exposedness. Here again, the measures can be decomposed in two categories, known under the name of full-reference [4], [15]–[18] and no-reference quality metrics [19]–[21].

For a detailed presentation of the cited papers, we refer to the supplementary material provided with this paper. For a more complete and general review of the quality assessment method we refer to [1], [22]–[24].

These numerous studies for image quality assessment and their divergent or even contradictory conclusions point to the lack of universally accepted definitions and measurements of image quality. All studies we mentioned are motivated by the emergence of more and more effective TMOs, applied to the richer content of an HDR image. This combination has introduced new degrees of freedom in image rendering. The new local TMOs are indeed incredibly flexible, and can at will enhance locally the image and manage its colors. Given these new degrees of freedom, the reviewed studies primarily aim at establishing quantitative aesthetic criteria to orient TMO’s and fix their parameters. The variety of image quality criteria indicates that they are subjective, culture-dependent. This is why they must be calibrated by subjects.

Our goal here is more restricted and focuses on the purely image processing side of the question. We intend to rank methods not by their final image aesthetic quality, but by what they are forbidden to deliver. In other words, a “good” TMO should be able to create tasty or tasteless exaggerated images as well. The goal of image processing here is rather to provide the maximal freedom to photographers and camera designers.

In short we have two separate problems. One is the aesthetic quality assessment of images produced by TMOs with well selected parameters. The other problem is to evaluate how freely

these parameters can be set without producing unacceptable image quality flaws (artifacts!).

Indeed, as will be confirmed in the next section, the main limitation to image operators is the artifacts they produce. Defining a correct artifact measure helps deciding which base+detail method has most degrees of freedom. Thus, this method will be the best, as it can more freely adapt to any imaging design.

Organization: This section is organized in two subsections. The first is devoted to the literature on artifacts, their discovery and measurement. The second subsection reviews how papers have addressed the challenging question of setting the parameters of each method in a comparison benchmark.

A. Existing description and measures of artifacts

While artifacts are the most frequent reason invoked to propose better algorithms, no serious attempt to define quantitatively and measure those artifacts has been proposed so far. The presence of the artifacts, on the other hand, is testified in a number of papers.

In [22] for example, the presence of artifacts in the local tone-mapping operator is invoked to explain why a number of studies conclude that global operators are preferred over the local ones. When Čadík *et al.* [25] included in their perceptual study² the notion of artifacts, it appeared that this attribute participated to a large extent to the global perceived quality.

Artifacts are often invoked as a reason to propose new base+detail decomposition filters. Furthermore, comparisons between base+detail filters are generally made on some difficult images that generate artifacts; so that comparing the filters amounts to comparing their artifacts. However, no exhaustive list of the artifacts has been proposed yet. This is problematic, as often a new method solves one artifact while introducing another one, which is later uncovered by another paper. This is the case for example for the weighted least squares filter (WLS) [26].

In this paper, Farbman *et al.* consider the problem of multi-scale detail enhancement. They show that former existing schemes produce artifacts: either a *staircase effect* in the scheme of Fattal *et al.* [27], or a *luminance halo* in the scheme of Chen *et al.* [28]. They then show that their proposed filter does not create any of these artifacts. As we shall see, their filter actually introduced a strong *compartmentalization* artifact, which would later be pointed out, for example in [29].

Chronologically, the next successful edge-aware smoothing filter is the guided filter (GF) [29]. In this paper, GF is compared against the bilateral filter (BF) [30]. The authors argue that their filter avoids *staircasing*, and an “intensity shift” artifact in WLS, which corresponds to what we shall call *compartmentalization*. Yet, GF was actually introducing a new artifact, the *contrast halo*.

In 2011, Gastal *et al.* proposed a fast filter called *domain transform* (DT) [31]. Its compartmentalization was not compared to that of previous filters. Yet DT produces it the most, as we shall see in Section VI. As for the contrast halo artifact

of GF, it was also precisely described in [32]. In short, the artifacts are known, sometimes under different names, and serve as reference for the comparisons. Yet, with the exception of the *luminance halo* there is no proposed measurement for each, and still less a joint measurement.

Of the four artifacts covered in this paper, the most known and most discussed one is unquestionably the luminance halo, often simply called *halo*. It has been studied by Trentacoste *et al.* [33] in 2012, where the authors analyzed its perception and wondered if it should be viewed as an enhancement or as an artifact. Both interpretations indeed coexist. The authors show that the decision between both depends on the halo’s amplitude and width. In this paper, the authors propose a contrast enhancement method based on countershading. They conducted a perceptual study to determine the parameters of their method, so that “local contrast can be introduced by [their] operator without becoming objectionable”. They modeled the objectionable threshold on the magnitude of the countershading profile in function of the standard-deviation of the Gaussian filter used to generate it. This unfortunately is specific to the Gaussian filter and does not allow to measure the luminance halo generated with other methods.

Li, Sharan and Adelson in 2005 [34] largely discuss the halo artifact, as they method is based on the multi-scale manipulation of Laplacian coefficients. They succeed in masking the luminance halo by choosing adequate weights; yet here again no attempt was made to measure it.

Jang *et al.* [35] proposed a method to automatically adjust the parameters of the multi-scale retinex algorithm, so as to optimize the perceptual quality of the contrast-enhanced image. A measure of the contrast was obtained using local standard-deviations. To set the weight and width of the Gaussian filters, they proposed a measure to evaluate the presence of halos on test images. The halo artifacts were evaluated based on the maximum difference between each pixel intensity on one side of the edge and the average intensity on the same side. The maximum intensity difference corresponding to each side of the edge is computed as

$$h_s = \max_{x \in \Omega_s} (|I(x) - \bar{I}|), \quad s \in \{\text{left}, \text{right}\}, \quad (1)$$

where Ω_s represents the pixels on the left or right side of the edge and \bar{I} represents the mean value. Finally, the overall halo artifact measure is obtained based on the averaged maximum intensity differences for each edge side:

$$H = \frac{1}{2}(h_{\text{left}} + h_{\text{right}}). \quad (2)$$

We shall use a similar measurement on our evaluation pattern.

B. Setting the parameters

In virtually every quality assessment paper, the authors have to decide how the parameters of the different tone-mapping operators will be fixed. Most of the time, they rely on the parameters given by the authors, but while this seems correct for TMOs with the same *intent*³, it does not make sense when the parameters were set with a different objective in mind. We refer to [36, Section 7.2.3] for a review of the different

²Described in supplementary material, section related work, subsection perceptual studies.

ways used in TMO evaluation for the parameter settings. In this book section, the authors consider three groups: 1) use of default parameters; 2) tuned by experts; 3) pilot study.

In their evaluation of TMOs for HDR-video in 2013 [3], Eilertsen *et al.* described an original way of setting the parameters of the tested operators. They asked four experts to tune the parameters so that they produce good results in three sequences, using Powell’s conjugate direction method, where at least two full iterations were completed. Finally the parameters obtained with the different experts were averaged and then used in two subjective evaluation experiments⁴. This process of manual tweaking can be helped by *perceptually linearizing* the parameter space [37].

All such methods rely on subjective evaluations of the final tone-mapped images. Our problem is different, for two reasons. First, there is no reference for the detail image; second, it is unclear what the best-looking detail layer would be, since this type of image is quite unnatural. In fact, we are not interested here in the subjective quality of the detail (nor of the enhanced images), but in the artifacts they may introduce for a comparable enhancement of the contrast. As said earlier, our concern is to evaluate the range in which a filter can be used without introducing objectionable artifacts. This amounts to evaluating the strength of artifacts when the filters produce the same amount of detail. In Section V we describe our method, which sets the parameters of each filter so that the average L^2 -norm of the detail layer is equal for each filter.

III. A LIST OF REPRESENTATIVE FILTERS

A. Criteria for the choice of the filters

We shall restrict ourselves to seven filters. Each one is an acknowledged representative of a wide class of filters. We list them together with their abbreviations.

- 1) the bilateral filter (BF),
- 2) the guided filter (GF),
- 3) the weighted least squares filter (WLS),
- 4) the local Laplacian filters (LLF),
- 5) the total variation with L^1 data fidelity (TV- L^1),
- 6) the image smoothing via L^0 gradient minimization (IS- L^0),
- 7) the domain transform (DT).

The classes of algorithms under consideration are quite different. The bilateral belongs to the wide class of neighborhood filters that perform a nonlinear local convolution. The guided filter belongs to the class of anisotropic filters. The weighted least squares filter derives from a variational edge aware model, the local Laplacian filter is wavelet based and inherently multiscale. The total variation is a functional analysis model, the L^0 and L^1 are sparsity models, and the domain transform has an underlying image+color manifold model.

These filters are representatives of different image structure models, which lead to a different notion of detail and therefore to different artifacts when the detail is enhanced.

³See supplementary material, section related work, subsection perceptual studies.

⁴Described in supplementary material.

The selected filters and their acronyms are listed in Table I, along with their parameters. The methodology we use to set the parameters is described in Section V. We shall now briefly present each filter with its definition and the artifacts it introduces⁵.

B. Presentation of the seven filters

1) *The bilateral filter*: First intended for denoising, this filter appeared in 1983 with Yaroslavsky [38] and Lee [39]. The variant using two Gaussian functions was proposed by Smith and Brady who called it “SUSAN” (1995) [40]. It was discovered again by Tomasi and Manduchi in 1998 [30] who named it “bilateral filter”. It is defined by

$$v(\mathbf{x}) = \frac{1}{C(\mathbf{x})} \sum_{\mathbf{y} \in \Omega} e^{-\frac{\|\mathbf{x}-\mathbf{y}\|^2}{2\sigma_s^2}} e^{-\frac{|u(\mathbf{y})-u(\mathbf{x})|^2}{2\sigma_r^2}} u(\mathbf{y}), \quad (3)$$

where u and v are the input and filtered images, respectively; \mathbf{x} and \mathbf{y} are pixels positions and Ω a window. C is the normalization factor. This filters has many variants, for example the joint bilateral filter and the unnormalized bilateral filter to name a few. Numerous fast approximations have been proposed. We refer to the Paris *et al.* book [41] for a thorough review. We shall consider in this paper the most representative of its fast approximations, namely, the bilateral grid [28], [42]. To avoid any artifact due to the approximation, the range subsampling will be set to be very fine, *i.e.*, $S = 64$ with S the number of slices, considering that the parameter $\sigma_r \simeq 0.1$ (image dynamic in $[0, 1]$).

2) *The domain transform* [31]: The idea of this fast filter is to make a nonlinear monotone domain transform on each image line so that the bilateral filter applied to each line boils down to a convolution. The image is then alternately filtered in line and in column to emulate a 2D bilateral filter. On each line the image coordinate z is redefined as a strictly increasing 1D signal $ct(z)$ by

$$ct(z) = \int_0^z 1 + \frac{\sigma_s}{\sigma_r} \sum_{k=1}^c |u_{x,k}(x)| dx, \quad (4)$$

where σ_r , σ_s are the filter’s parameters and $u_{x,k}$ is the derivative of the input image u for channel k and pixel x . This amounts to defining the new distance between image points 0 and z as the geodesic distance between $(0, u(0))$ and $(z, u(z))$ in the image graph. As a result, pixels with distant intensities fall apart. Hence, a Gaussian filter applied on the transform domain averages them but little.

3) *The guided filter* [29]: This filter, ubiquitous in image processing since its publication in 2010, is defined by

$$\text{GF}\{u\}(\mathbf{x}) = \bar{a}(\mathbf{x})v(\mathbf{x}) + \bar{b}(\mathbf{x}), \quad (5)$$

⁵More filters are presented in supplementary material: those that we do not consider because they would be redundant or are too complex, and others that directly modify the local contrast without base+detail decomposition.

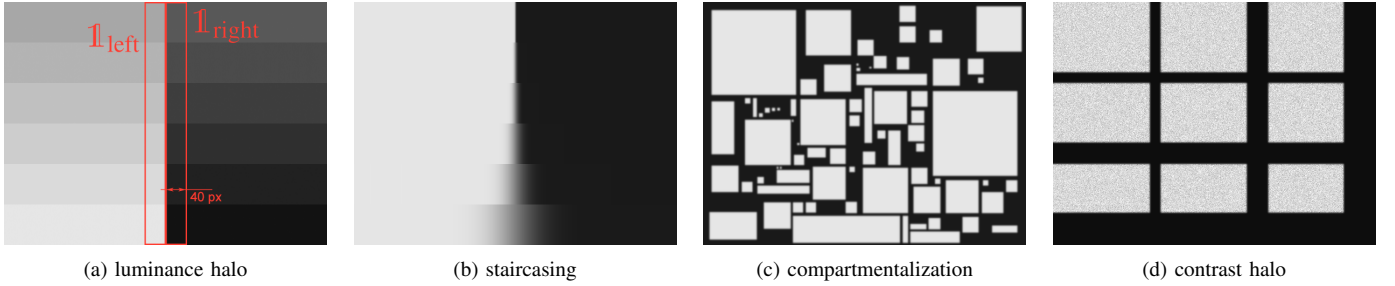


Figure 2. Test patterns for artifacts measurements. The first two patterns (a) and (b) are in fact a series of 6 patterns composed of one single vertical edge, as explained in section IV-A. We display here for these two patterns a stack of horizontal bands taken from each of the input.

where the bar $\bar{\cdot}$ means a mean in the neighborhood defined by a square window Ω and the linear coefficients a and b are obtained by minimizing the cost function

$$E(a(\mathbf{y}), b(\mathbf{y})) = \sum_{\mathbf{x} \in \Omega(\mathbf{y})} \left((a(\mathbf{y})v(\mathbf{x}) + b(\mathbf{y}) - u(\mathbf{x}))^2 + \epsilon a(\mathbf{y})^2 \right), \quad (6)$$

where ϵ is the smoothing parameter, $u(\mathbf{x})$ the original image and $v(\mathbf{x})$ the guide.

4) *The weighted least squares filter (WLS) [26]*: Given an input image u , this energy-based filter seeks an output v ,

which, on the one hand, is as close as possible to u , and, on the other hand as smooth as possible everywhere, except across significant gradients in u .

This translates into finding an image v minimizing

$$\sum_{\mathbf{x}} \left((v(\mathbf{x}) - u(\mathbf{x}))^2 + \lambda \sum_{z \in \{x, y\}} a_z(u, \mathbf{x}) \left(\frac{\partial v}{\partial z} \right)^2(\mathbf{x}) \right), \quad (7)$$

where $a_x(u, \mathbf{x})$ and $a_y(u, \mathbf{x})$ are smoothness weights defined as

$$a_z(u, \mathbf{x}) = \left(\left| \frac{\partial \ell}{\partial z}(\mathbf{x}) \right|^\alpha + \epsilon \right)^{-1}, \quad (8)$$

where ℓ is the *log-luminance* channel of u .

5) *The local Laplacian filter [43]*: This filter is considered as the highest quality base and detail decomposition, to the price of a higher complexity. Although inspired from the bilateral filter, it presents almost no staircase effect. This filter is versatile and can be used for a wide variety of contrast manipulations tasks, ranging from edge-aware smoothing to local contrast enhancement with dynamic reduction. It directly computes the Laplacian pyramid of the output image; a final operation collapses the pyramid and builds the filtered image. Each Laplacian coefficient is computed independently using a dedicated *remapping function*, which shape is chosen in function of the application. The fast version (FLL) uses the Durand-Dorsey [44] slicing strategy. It greatly speeds up the execution by computing only a reduced number of remapped images.

The filter can be summarized in the next formula,

$$Lpyr\{v, l\}(\mathbf{x}) = \sum_{i=1}^S A_i(l, \mathbf{x}) Lpyr\{u'_i, l\}(\mathbf{x}), \quad (9)$$

where $Lpyr\{v\}$ is the Laplacian pyramid of the output image v , l is the scale, \mathbf{x} is a pixel, u is the input image and u'_i

the input remapped for the sample $i \in \{1, 2, \dots, S\}$. A_i is a weight map of the same size as $Lpyr\{u'_i, l\}$. The final image v is obtained by *collapsing* the constructed pyramid [45].

6) *Total variation*: The total variation model assumes that the total variation of the base is bounded while the detail would be highly oscillatory and therefore only integrable. This leads to a TV+ L^1 minimization which is classically performed by the Chambolle-Pock method [46], as implemented in [47]. This filter finds v minimizing

$$\|u - v\|_1 + \lambda \|\nabla v\|_1, \quad (10)$$

where λ is the smoothing parameter, u the input image, v the smoothed one (the base layer) and $u - v$ the detail layer. This filter was designed for the cartoon+texture decomposition introduced by Meyer [48].

7) *Image smoothing via L^0 gradient minimization*: This successful edge-aware smoothing filter proposed by Xu *et al.* [49] is based on the minimization of the L^0 norm of the gradients of the output image v . We shall call it IS- L^0 in the following. It consists in minimizing the number of non-zero gradients while ensuring that the output stays close enough to the original image with a quadratic data attachment term. Formally, the method seeks an image v that minimizes

$$\|u - v\|_2^2 + \lambda C(v), \quad (11)$$

where $C()$ counts the number of pixels whose gradient is not zero, and λ is a parameter that controls the amount of smoothing. The second term requires the base's gradient to be sparse.

IV. THE MAIN ARTIFACTS AND THEIR TEST PATTERNS

In this section we present the measures designed to quantitatively evaluate the four canonical artifacts of edge-aware filters. Each measure is associated with a test-pattern specifically designed to detect and measure one of the artifacts. This evaluation is limited to the artifacts representing the main impediments in the base+detail filters. They are the *luminance halo*, the *staircasing*, the *compartmentalization* and the *contrast halo*. The corresponding test-patterns are displayed in Figure 2. For each artifact, we shall point out the filters that produce them most.

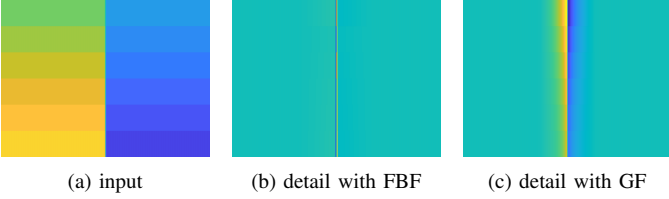


Figure 3. Luminance halo artifacts with GF. This triptych presents bands of the input patterns in (a), bands of the detail layers obtained with FBF, which has no luminance halo (b), and bands of the detail layers obtained with GF which has the highest halo score (c). All of these images are represented with false colors. Dynamic range is $[0, 1]$ for (a) and $[-0.04, +0.04]$ in (b) and (c).

A. The luminance halo

The luminance halo is the most common artifact of contrast enhancement filters, already present in high pass filters. It arises when a contrasted edge has been smoothed, even slightly, while it should have been preserved in the base.

To measure the luminance halo, it is enough to build a test-pattern containing flat regions separated by straight edges of all amplitudes. The measure then simply quantifies the distance between the filtered image and the input one.

a) Test-pattern: For this pattern, as well as for the staircase effect test pattern (described in IV-B (a)) we actually use a series of six patterns. This is because we have two contradictory needs. First, we need to test different edge heights. Yet we also need to dispose of patterns with only one edge. Indeed, this ensures that the deformation caused by the filter (the artifacts!) does not come from another nearby edge. The six patterns have a centered vertical edge with different heights (we used $\{0.3, 0.4, 0.5, 0.6, 0.7, 0.8\}$ for this pattern). Each pattern is filtered with the tested filter, then a horizontal band (with the same width but only one 6th of the initial height) is extracted in the middle of the pattern. The 6 bands are stacked together to create a single output image. This composite base layer is then used for the halo measurement. This explains why the detail layers only display horizontal luminance halos (for example in Figure 3 (c)).

b) The halo measure: Based upon this test-pattern, the halo measure is defined by

$$\mathcal{H}(u_0, u_1) = \sum_{\mathbf{x} \in \Omega} \mathbb{1}_{\text{left}}(\mathbf{x}) \left((u_0(\mathbf{x}) - u_1(\mathbf{x}))^+ \right)^2 + \sum_{\mathbf{x} \in \Omega} \mathbb{1}_{\text{right}}(\mathbf{x}) \left((u_1(\mathbf{x}) - u_0(\mathbf{x}))^+ \right)^2, \quad (12)$$

where \mathbf{x} is a pixel, u_0 is the input image, u_1 is the filtered image and $\mathbb{1}_{\text{left}}$, $\mathbb{1}_{\text{right}}$ are indicator functions. These functions equal 1 in rectangles of width 40 pixels (the standard-deviation of the tested filters) and are placed on the left and right side of the vertical edge respectively. The rectangles are displayed in Figure 2 (a). We denote by Ω the image domain and $(\cdot)^+$ denotes the positive part. Because a few strong differences are more annoying than numerous small ones, we square the positive part in Equation (12).

c) Which filter performs worst: The worst filter for the luminance halo artifact is the guided filter. Figure 3 shows

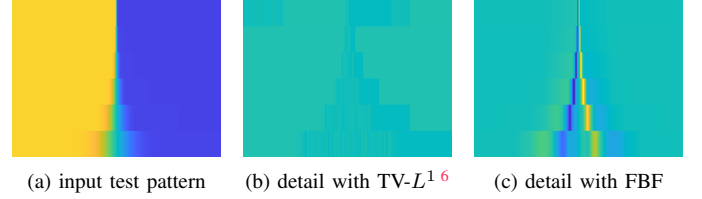


Figure 4. Staircasing test pattern (a). Detail layer with TV-L^1 which gives the smallest score and with FBF which gives the highest. The input test pattern (a) and its decomposition are represented with false colors. Dynamic range is $[0, 1]$ for (a) and $[-0.1, +0.1]$ in (b) and (c).

the detail layer given by this filter for our test-pattern, and compare it to the detail layer obtained with the fast bilateral filter, which creates the least luminance halo. The parameters of both filters are given in Table I.

B. The staircase effect

The staircase effect is typically present in the bilateral filters; it is sometimes referred to as an edge sharpening effect. Since the sign of the edge’s gradient in the detail layer is opposite to its sign in the input image, enhancing the detail causes “gradient reversal” in the final detail-enhanced image, which is yet another way to refer to this artifact. Numerous correction schemes have been proposed [41] but often fail at effectively correcting this artifact; even the bilateral filter with regression [50] that has been proposed specifically to solve this artifact can present it in some conditions such as a large spatial support.

a) The staircasing test-pattern: Like in the luminance halo pattern which construction is described in section IV-A, we use a set of six images to measure the staircase effect. This allows us to filter images which contain only one (smooth) edge but to test several edge widths. Each of the six input pattern has a contrasted and blurred vertical edge. The patterns are generated using a step edge convolved with a Gaussian kernel in the Fourier domain using the standard-deviation $\sigma = \{0.7, 1.4, 2.8, 5.6, 11.2, 22.4\}$. Similarly to the luminance halo, we display a preview of the input patterns by piling up horizontal bands into a single image shown in Figure 2 (b). The same process is used after filtering with a tested filter so as to create a single output containing the six blurred edges. This output is then used for the measurement. This construction explains why the merged filtered image shows no interaction between the bands; see Figure 4 (b) and (c).

b) The staircase measure: Using the test-pattern we just described, we measure the edge reinforcement in the six bands simultaneously using

$$\mathcal{S}(u_0, u_1) = \sum_{\mathbf{x} \in \Omega} \mathbb{1}_{\text{left}}(\mathbf{x}) \left((u_1(\mathbf{x}) - u_0(\mathbf{x}))^+ \right)^2 + \sum_{\mathbf{x} \in \Omega} \mathbb{1}_{\text{right}}(\mathbf{x}) \left((u_0(\mathbf{x}) - u_1(\mathbf{x}))^+ \right)^2, \quad (13)$$

⁶Horizontal oscillations with amplitude 1 appear in TV-L^1 results. This is due to the conversion from double to unsigned 8-bits integer needed in the implementation we used. This is not due to the algorithm itself, and has a negligible influence on the measures.

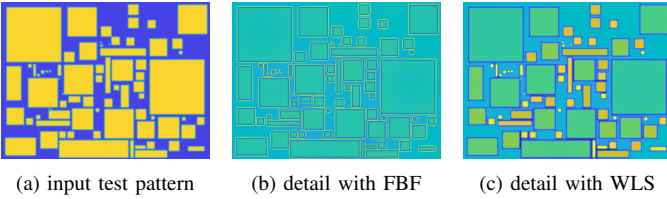


Figure 5. This triptych shows the compartmentalization test pattern (a), the detail layer obtained with the lowest score filter FBF (b), and with one of the highest score filters, WLS (c). All images are represented with false colors. Dynamic range is $[0, 1]$ for (a) and $[-0.1, +0.1]$ in (b) and (c).

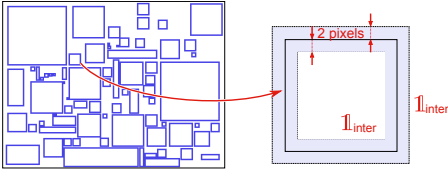


Figure 6. Illustration of the mask used in the compartmentalization measure: in order to quantify the alterations of the bright areas inside the shapes and the alteration of the dark interstices, we measure the variance of the detail layer using the mask $\mathbb{1}_{\text{inter}}$ displayed in white in the figure. A two pixels wide area (the blue regions) is excluded on the inner and outer borders of the shapes, because of the slight smoothing we applied to avoid aliasing.

where the indicator functions $\mathbb{1}_{\text{left}}$ and $\mathbb{1}_{\text{right}}$ are the same as for the luminance halo. They are displayed in Figure 2 (a) and presented in Section IV-A.

c) *Worst filters*: The worst filters are the bilateral filter and, without surprise, the L^0 gradient minimization filter. We display in Figure 4 (c) the detail layer obtained with FBF. On the detail image, the artifact appears as blue bands on the left side of the edge and yellow bands on the right side. The increasing width of the edge allows to determine the scale at which the artifact appears. The worst case is always the finest edge, but the attenuation when the edge width increases depends on the filter. As control, we show the detail layer obtained with $\text{TV-}L^1$, which has no staircase effect⁷.

C. The compartmentalization effect

The compartmentalization effect arises when a constant color region (typically a wall, or the sky) is compartmented into pieces with variable size by the superposition of a grid, or of tree branches, etc. The artifact consists in an intensity shift of the detail in constant regions; its magnitude depends on the area of the region. The smaller the region, the stronger the artifact. The total variation [51], [52] presents a drastic compartmentalization: it removes local extrema with small area from the base and puts them fully in the detail, while the larger extremal regions are left in the base.

a) *The compartmentalization test-pattern*: The compartmentalization test-pattern is made of bright squares and rectangles of different areas disposed on a dark background (Figure 2). This image is slightly smoothed to avoid aliasing.

b) *The compartmentalization measure*: Using the test-pattern described above, the measure is defined by

$$\mathcal{P}(u_0, u_1) = \text{var} \{ (u_0 - u_1) \mathbb{1}_{\text{inter}} \} \quad (14)$$

⁷The detail layers obtained with the different filters are observable in the supplementary materials.

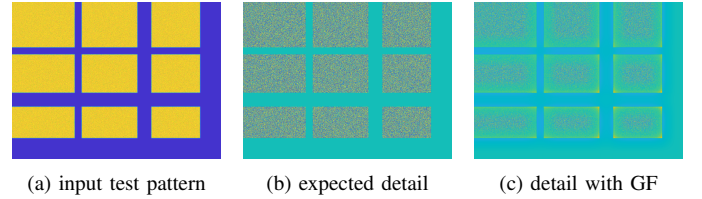


Figure 7. Contrast halo pattern (a); expected detail layer (b), which contains only the noise of the test-pattern; result obtained with GF (c), which gives the strongest contrast halo score. All images are displayed with false colors. Dynamic range is $[0, 1]$ for (a) and $[-0.1, +0.1]$ for (b) and (c).

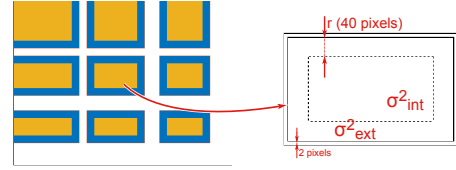


Figure 8. Masks used in the contrast halo measure. The variance σ_{ext}^2 is computed in the blue areas and the variance σ_{int}^2 in the yellow ones. The red lines show the excluded pixels on the borders of the rectangles. The white area is not used in the measure.

where $\mathbb{1}_{\text{inter}}$ is a mask corresponding to the image deprived of a 2-pixels wide band along the inner and outer borders of the shapes. This excludes pixels influenced by the edge. This mask appears in white in the illustration of Figure 6. The removed pixels in the squares are shown in blue.

c) *Filters with worst compartmentalization*: A filter with spectacular compartmentalization artifacts is WLS. Figure 5 displays the result obtained with this filter using the parameters set in Section V and compares it to the detail layer obtained with FBF, which does not have compartmentalization in (b). One can recognize the staircase effect in image (b) but the edges are not taken into account in the measure. Thus they do not influence the compartmentalization score. With the false colors used, the bright regions appear in yellow and the dark ones in blue; in the detail layer in (c), one can clearly see that WLS “lights up” the small shapes. The small interstices between the rectangles are affected by the compartmentalization effect too; they appear as darkened zones in (c). Our measure takes it into account. The highest score for the compartmentalization, however, is not obtained by WLS but by the domain transform filter⁸. Yet the compartmentalization present in DT is related to its luminance halo artifact; in fact edges are not well preserved by this filter, which causes the small elements to be smoothed out even if their contrast is high. Thus, all shapes in the test-pattern are affected. For filters like WLS however, there is a distinct separation between shapes that are affected (those that are lit in the detail layer) and those that are not.

D. Contrast halo

The contrast halo appears when regions containing details and close to edges are not filtered. This artifact is typical of the guided filter.

⁸The detail layers obtained with the different filters are observable in the supplementary material.

a) *Test-pattern for the contrast halo*: This test-pattern consists in a texture (noise) surrounded by contrasted edges with different widths. We display it in Figure 2 and with false colors in Figure 7 (a).

b) *Measure*: Using the test-pattern described above, the contrast halo is measured by comparing the variance of the detail layer in the interior of the bright rectangles with the variance on the border of these rectangles, as shown in Figure 8. Because of the luminance halo, this ratio can sometimes be inferior to 1, *i.e.*, the variance in the exterior side of the bright rectangles becomes higher than in the interior. We thus simply measure the maximum of 1 and of their ratio. Formally, this gives

$$\mathcal{C}(u_0, u_1) = \max \{1, \sigma_{\text{int}}^2 / \sigma_{\text{ext}}^2\} - 1, \quad (15)$$

where the subtraction of 1 only aims at giving the same minimum to \mathcal{C} as to the other measures, which will be useful in the final comparison. The two measures of variances are obtained thanks to masks, displayed in Figure 8. The value of σ_{ext}^2 is measured in the blue regions and σ_{int}^2 in the yellow ones.

c) *Filters with worst contrast halo*: The guided filter is the only filter among the tested ones that have a contrast halo artifact. The Figure 7 (c) shows the filtering result on this dedicated test-pattern: the texture is hardly removed near the dark barriers. We provide as reference a synthetic detail layer we expect to be extracted by the filters. It contains only the noise of the test-pattern (a).

V. SETTING THE PARAMETERS OF EACH FILTER

In this section we discuss how to set fair parameters for each filter. When we shall compare in Section VI the strengths of their respective artifacts, it is of prime importance to ensure that they are compared in a condition where they deliver similar contrast enhancement.

Using the default parameters given by the authors wouldn't be right. Notably, a cautious filter might cause less visible artifacts, but the detail enhancement might be insufficient by then. Our problem is thus to obtain similar amounts of detail.

We therefore propose to equalize the L^2 -norm of the detail layer.

The methodology we propose can be characterized as semi-automatic. For each filter, we set all parameters using two basic rules, and the last and more important one is set automatically. The rules are simply (1) to use default values suggested by the authors when possible, while (2) ensuring a coherence between the different filters. For example, if available, parameters that control the spatial scale of the detail extraction are set to the same value. The last parameter set automatically is the one that controls the amount of detail. This parameter is set so that the average L^2 -norm of the detail layer on a small set of images is the same for each filter. The five images we used are displayed in Figure 9. They were chosen so as to present real-life cases with a standard balance of texture and edges.

To avoid penalizing smaller images, we preferred to equalize the PSNR (Peak Signal to Noise Ratio) of the images, because it is independent of their size,

$$\text{PSNR}(u_0 - u_1) = -10 \times \log_{10} \left(\frac{1}{\sqrt{N}} \|u_0 - u_1\|_2 \right), \quad (16)$$

where N is the number of pixels in the image. The PSNR was measured on each image filtered with the current parameter, then averaged. For the cross-calibration of all filters we fixed the target at PSNR = 16.23 dB, which corresponds to a decent amount of detail for all filters.

We list in Table I the fixed parameters and give in the last column the parameters obtained with our procedure⁹.

VI. MEASURING THE ARTIFACTS

In this section, we measure the strength of each of the four artifacts presented above. A table will display the results for all the filters listed above. Our method is simple: for each filter, using the parameters given in Table I, we measured the tested artifact using equations given in Section IV. We give in Figure 10 four bar plots presenting the values \mathcal{H} , \mathcal{S} , \mathcal{P} and \mathcal{C} for each filter, sorted in descending order¹⁰. The smaller the value, the better the filter; this way the filters are directly ranked.

In the first Section VI-A, we comment and explain the results. In a second Section VI-B, we make a summary of the five tables. We propose a method to merge the independent scores into a single value that summarizes the ability of the filter to perform a clean base+detail decomposition and deliver the final ranking. This ranking is confirmed by a rejection table summarizing the experts' evaluation of artifacts. The last Section VI-C summarize and concludes on our results.

A. Artifact-wise measures and ranking

a) *Luminance halo*: The worst filters in this case are IS- L^0 and GF¹¹.

b) *The staircase effect*: Once again IS- L^0 is the worst filter¹²: indeed, minimizing the L^0 norm of the gradients tends to create constant parts in the image, which creates a staircase effect. Unsurprisingly, the (fast) bilateral filter comes next after IS- L^0 . This artifact of the bilateral filter has long been known [50]. The weighted least squares filter has, to a certain extent, this artifact too, with the particularity that it is way more marked in the dark side of the halo. This is due to the use of a logarithm in the gradient penalization: dark parts of the images are allowed to move more than the bright ones.

c) *The compartmentalization artifact*: The expected detail is a constant image: indeed, the test-pattern does not contain texture, but only very contrasted edges. On the contrary, filters with compartmentalization tend to darken the background stripes separating the rectangles and to "light up"

⁹The detail layers obtained with these parameters for the images in Figure 9 are presented in the supplementary material.

¹⁰The detail layers obtained with the different filters for each pattern are observable in the supplementary materials.

¹¹See Footnote 10

¹²See Footnote 10.



Figure 9. Images used to set the parameters of all methods.

Table I
TESTED FILTERS AND THEIR PARAMETERS

Abbreviation	Algorithm	Fixed	Set
GF	Guided filter [29], [53]	$r = 40$	$\epsilon = .075^2$
FBF	Fast bilateral filter (bilateral grid) [28], [54]. Number of intensity samples: $S = 64$	$\sigma_s = 40$	$\sigma_r = .1178$
DT	Domain transform [31]. Using the recursive filter and 3 iterations	$\sigma_s = 40$	$\sigma_r = 0.1166$
WLS	Weighted Least Squares [26]. Guide image ℓ set to default: log-luminance of input u	$\alpha = 1.2$	$\lambda = 0.5$
FLL	Fast local Laplacian filter [55]. Number of samples for range subsampling: $S = 64$	$l_{\max} = 6$	$\sigma_r = 0.103$
TV- L^1	Total variation using L^1 norm [47]	-	$\lambda = .205$
IS- L^0	L^0 image smoothing [49]	$\kappa = 2$	$\lambda = .002$

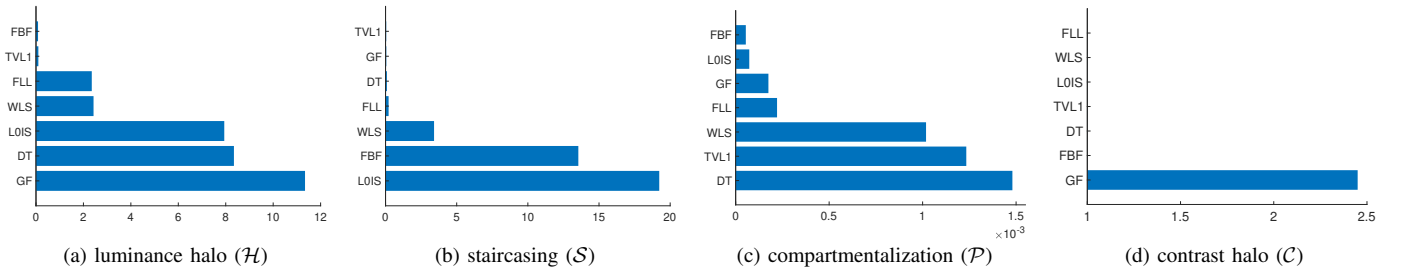


Figure 10. Objective measures of the artifacts. For each plot the filters are ranked according to their score. The lower the better.

some of the squares or rectangles of the test-pattern in function of their area. The worst result for this measure is obtained with the domain transform (DT), that tends to smooth out the small objects whatever their contrast¹³. Note that contrarily to WLS that lights up only some shapes in function of their areas, DT affects every shape. So for this filter the compartmentalization is linked to the luminance halo. As expected, WLS has a very high score too. This is explainable because even the edges see their gradients slightly penalized. Thus it becomes sometimes worthy, in terms of energy minimization, to reduce those edges if the area inside is small enough, because the data term, having few pixels, will not compensate the gain. The second worst filter is TV- L^1 . Indeed, this filter is prone to removing the edges of objects and “closing” regions with small area. Next, IS- L^0 also has a bad score, for the same reason as presented in the luminance halo paragraph. In its case the compartmentalization is not really annoying because it seems to affect the shapes whatever their area. Other non-zero results are mainly due to the luminance halo, to which our test-pattern cannot be completely insensitive. Note also that the “contour highlighting” visible in FBF, BFR and IS- L^0 is due to the staircase effect. This, however, does not influence the value of our measurement.

d) *The contrast halo results:* As explained in Section IV, with this test-pattern we aim at measuring if the detail is affected in the vicinity of an edge. Put another way, we

measure if the smoothing is the same in the vicinity of edges as at a certain distance from it. The filter that obtains the highest and therefore worst score is the guided filter¹⁴. Its detail layer is displayed in Figure 7, along with the guided filter’s result.

B. Final score and ranking

Merging the different measures may look problematic for three main reasons:

- 1) the perceived nuisance of an artifact is non-linear;
- 2) the artifacts are not equally disturbing;
- 3) our measures have ranges that are not comparable.

When global quality assessment scores are available, one can overcome these difficulties by performing a polynomial regression. This method has been used for example in the context of tone-mapped images quality assessment [7], [25] to merge different quality measures and try to approximate the subjective response of a large number of non-expert subjects¹⁵.

We, however, worked with five experts at DxO, as the evaluation given by photography experts is much more reliable. It actually also relies on the feedback of many amateur photographers. Rather than attributing global notes to the filters, we intend to detect objectionable artifacts in the filters. This rating method is similar to [15], [33], that identified objectionable thresholds using perceptual studies.

¹⁴See Footnote 10.

¹⁵See the supplementary material.

¹³See Footnote 10.

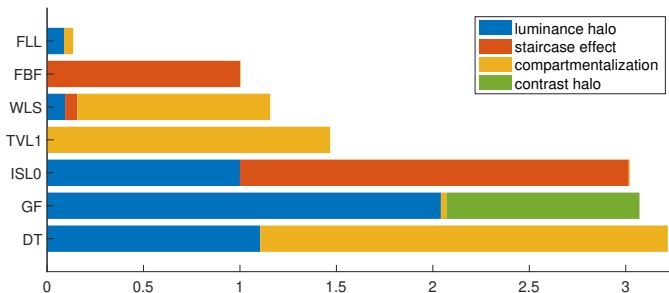


Figure 11. Comparison and ranking of the fused scores \mathcal{A} obtained with Equation (17). The lower the better.

These experts were asked for a clear cut categorization of each triplet (image, filter, artifact) in two classes: *non-objectionable*, and *objectionable*. The experiment was carried-out on contrast enhanced images with a high factor on the detail. The comparison was performed by flipping between the input images provided for reference and the enhanced ones. The set of images was partly composed of the examples displayed in Figure 9, completed with 10 other challenging images from DxO database. They were asked in the end to make a decision for the couple (filter, artifact) that summarizes their observations, so that we obtained a rejection table for every expert. We then merged the tables. To secure an objectionable decision, we marked the couple (filter, artifact) as rejected only if at least four of the five judges marked them as objectionable. We provide in Table II the result of their judgment.

For each tested filter, Table II fixes its objectionable artifacts. We shall only use this expert rating to fix a threshold for the artifact’s score. The value we seek lies between the largest non-objectionable score and the smallest objectionable one. We chose to use the smallest objectionable score as threshold for each artifact. This score is therefore associated with one of our seven filters. Hence, using our measures in Figure 10 and Table II, we have that

- IS- L^0 defines the score threshold for the luminance halo,
- FBF defines the score threshold for the staircasing,
- WLS defines the score threshold for the compartmentalization,
- GF defines the score threshold for the contrast halo.

The scores of these filters are then used to normalize the measures. This provides a workable solution to the two last difficulties listed above. Concerning the first difficulty, we chose to square the artifact measures. This makes the objectionable scores more discriminant and the acceptable ones less impacting, and translates in the simple fusion equation:

$$\mathcal{A}(f) = \frac{\mathcal{H}(f)^2}{\mathcal{H}(\text{IS-}L^0)^2} + \frac{\mathcal{S}(f)^2}{\mathcal{S}(\text{FBF})^2} + \frac{\mathcal{P}(f)^2}{\mathcal{P}(\text{WLS})^2} + \frac{\mathcal{C}(f)^2}{\mathcal{C}(\text{GF})^2}, \quad (17)$$

where f is a filter and $\mathcal{A}(f)$ its final score taking into account the four artifacts. The fused measures are compared (and sorted) in Figure 11.

C. Summary and conclusion on the comparative experiments

We find in the fused scores in Figure 11 that the fast local Laplacian filter (FLL) is the best and the domain transform

(DT), image smoothing with L^0 gradient minimization (IS- L^0) and the guided filter (GF) are the worst of the tested methods.

This is in excellent agreement with the experts’ rejection decisions. In Table II, each test-pattern disqualifies at least one method:

- the staircase effect invalidated IS- L^0 and FBF;
- the compartmentalization invalidated DT, TV- L^1 , WLS;
- the contrast halo invalidated GF;
- the luminance halo invalidated DT, GF, and IS- L^0 .

Only LLF succeeded passing the five artifact tests. Thus, this classification confirms the podium obtained in Figure 11, where the first place is attributed to the same filter. Furthermore, the 2nd, 3rd and 4th filters are the ones with only one objectionable artifact. All remaining filters suffer from two intolerable artifacts and get the last positions in the ranking.

VII. CONCLUSION

The emergence of more and more effective TMOs, applied to the richer content of an HDR image has introduced new degrees of freedom in image rendering. One of the sources of this incredible flexibility is the recent invention of powerful base and detail decomposition filters, that lie at the heart of local contrast manipulation methods. The multiplication of methods requires a quality measurement, independent of questionable aesthetic criteria.

We proposed an objective measure of the presence of artifacts in the base and detail decomposition filters. This involves several important contributions: the definition and measurement of four artifacts using *ad hoc* test-patterns, a methodology to set the parameters of the filters and the proposition of an unprecedented way to fuse the independent measures in a single quality mark. Our procedure evaluates the filters according to criteria that faithfully reflect the photographers’ requirements and are easily applicable to any base+detail filter.

Beyond the ranking of existing methods, we believe that our protocol can serve the design of new filters and the tuning of their parameters. The quantitative evaluation of success is a simple tool that can validate or invalidate any new proposed method.

Although we obtained for each artifact an expert acceptability threshold, we believe that our evaluation could become still more precise with a perceptual evaluation of a greater breadth.

An interesting direction for future works would be to extend our method to all contrast enhancement filters, not only those that explicitly produce a base and a detail layer. The difficulty remaining is to define an objective cross-calibration applicable to all such filters, so as to compare them all for a prefixed amount of enhancement.

ACKNOWLEDGMENTS

Work partly financed by Office of Naval research grant N00014-17-1-2552, DGA Astrid project « filmer la Terre » n° ANR-17-ASTR-0013-01. Charles Hessel’s Ph.D. scholarship was supported by a CIFRE scholarship of the French Ministry for Higher Studies, Research and Innovation. He wishes to thank his DxO collaborators Gabriele Facciolo, Wolf Hauser,

Table II
UNACCEPTABLE ARTIFACTS (IN RED) IN THE TESTED FILTERS.

	DT	IS- L^0	FBF	FLL	GF	TV- L^1	WLS
staircase effect							
compartmentalization							
contrast halo							
luminance halo							

Quoc Bao Do, Benoît Chauville, Frédéric Guichard for many valuable conversations and advice.

REFERENCES

- [1] E. Reinhard, W. Heidrich, P. Debevec, S. Pattanaik, G. Ward, and K. Myszkowski, *High dynamic range imaging: acquisition, display, and image-based lighting*. Morgan Kaufmann, 2010. 2
- [2] F. Drago, K. Myszkowski, T. Annen, and N. Chiba, "Adaptive Logarithmic Mapping For Displaying High Contrast Scenes," *Computer Graphics Forum*, vol. 22, no. 3, pp. 419–426, sep 2003. [Online]. Available: <http://doi.wiley.com/10.1111/1467-8659.00689> 2
- [3] G. Eilertsen, R. K. Mantiuk, R. K. Mantiuk, and J. Unger, "Evaluation of Tone Mapping Operators for HDR-Video," *Computer Graphics Forum*, vol. 32, no. 7, pp. 275–284, oct 2013. [Online]. Available: <http://doi.wiley.com/10.1111/cgf.12235> 2, 4
- [4] G. Eilertsen, R. K. Mantiuk, and J. Unger, "A comparative review of tone-mapping algorithms for high dynamic range video," *Computer Graphics Forum*, vol. 36, no. 2, pp. 565–592, may 2017. [Online]. Available: <http://doi.wiley.com/10.1111/cgf.13148> 2
- [5] A. Yoshida, V. Blanz, K. Myszkowski, and H.-P. Seidel, "Perceptual evaluation of tone mapping operators with real-world scenes," in *Proceedings of SPIE, Human Vision and Electronic Imaging X*, B. E. Rogowitz, T. N. Pappas, and S. J. Daly, Eds., vol. 5666, mar 2005, p. 192. [Online]. Available: <http://proceedings.spiedigitallibrary.org/proceeding.aspx?doi=10.1117/12.587782> 2
- [6] P. Ledda, A. Chalmers, T. Troscianko, and H. Seetzen, "Evaluation of tone mapping operators using a High Dynamic Range display," *ACM Transactions on Graphics*, vol. 24, no. 3, p. 640, jul 2005. [Online]. Available: <http://portal.acm.org/citation.cfm?doid=1073204.1073242> 2
- [7] M. Čadík, M. Wimmer, L. Neumann, and A. Artusi, "Image attributes and quality for evaluation of tone mapping operators," in *Proceedings of the 14th Pacific Conference on Computer Graphics and Applications*. Taipei, Taiwan: National Taiwan University Press, 2006, pp. 35–44. 2, 9
- [8] J. Kuang, H. Yamaguchi, C. Liu, G. M. Johnson, and M. D. Fairchild, "Evaluating HDR rendering algorithms," *ACM Transactions on Applied Perception*, vol. 4, no. 2, pp. 9–es, jul 2007. [Online]. Available: <http://portal.acm.org/citation.cfm?doid=1265957.1265958> 2
- [9] J. Kuang, R. Heckaman, and M. D. Fairchild, "Evaluation of HDR tone-mapping algorithms using a high-dynamic-range display to emulate real scenes," *Journal of the Society for Information Display*, vol. 18, no. 7, p. 461, 2010. [Online]. Available: <http://doi.wiley.com/10.1889/1.1828693> 2
- [10] F. Drago, W. L. Martens, K. Myszkowski, and H.-P. Seidel, "Perceptual evaluation of tone mapping operators with regard to similarity and preference," Max Planck Institut Fur Informatik, Stuhlsatzenhausweg 85, 66123 Saarbrücken, Germany, Tech. Rep. 2, 2002. 2
- [11] —, "Perceptual evaluation of tone mapping operators," in *ACM SIGGRAPH 2003 Sketches & Applications*. ACM, 2003, pp. 1–1. 2
- [12] J. Kuang, H. Yamaguchi, G. M. Johnson, and M. D. Fairchild, "Testing hdr image rendering algorithms," in *Color and Imaging Conference*, vol. 2004, no. 1. Society for Imaging Science and Technology, 2004, pp. 315–320. 2
- [13] J. Kuang, G. M. Johnson, and M. D. Fairchild, "Image preference scaling for hdr image rendering," in *Color and Imaging Conference*, vol. 2005, no. 1. Society for Imaging Science and Technology, 2005, pp. 8–13. 2
- [14] A. O. Akyüz, R. Fleming, B. E. Riecke, E. Reinhard, and H. H. Bühlhoff, "Do HDR displays support LDR content?" *ACM Transactions on Graphics*, vol. 26, no. 3, p. 38, jul 2007. [Online]. Available: <http://portal.acm.org/citation.cfm?doid=1276377.1276425> 2
- [15] T. O. Aydin, R. Mantiuk, K. Myszkowski, and H.-P. Seidel, "Dynamic range independent image quality assessment," *ACM Trans. Graph.*, vol. 27, pp. 69:1–69:10, Aug. 2008. [Online]. Available: <http://doi.acm.org/10.1145/1360612.1360668> 2, 9
- [16] H. Yeganeh and Z. Wang, "Objective assessment of tone mapping algorithms," in *2010 IEEE International Conference on Image Processing*. IEEE, sep 2010, pp. 2477–2480. [Online]. Available: <http://ieeexplore.ieee.org/document/5651778/> 2
- [17] —, "Objective quality assessment of tone-mapped images," *IEEE Transactions on Image Processing*, vol. 22, no. 2, pp. 657–667, 2013. [Online]. Available: https://ece.uwaterloo.ca/~z70wang/publications/TIP_{}_TMQI.pdf 2
- [18] R. Mantiuk, K. J. Kim, A. G. Rempel, and W. Heidrich, "HDR-VDP-2: A calibrated visual metric for visibility and quality predictions in all luminance conditions," in *ACM SIGGRAPH 2011 papers on - SIGGRAPH '11*, vol. 1, no. 212. New York, New York, USA: ACM Press, 2011, p. 1. [Online]. Available: <http://portal.acm.org/citation.cfm?doid=1964921.1964935> 2
- [19] T. O. Aydin, A. Smolic, and M. Gross, "Automated aesthetic analysis of photographic images," *IEEE Transactions on Visualization and Computer Graphics*, vol. 21, no. 1, pp. 31–42, 2015. [Online]. Available: <https://pdfs.semanticscholar.org/3396/f8eb0439d780d173c108cca7ba01e69f0cbc.pdf> 2
- [20] T. Mertens, J. Kautz, and F. Van Reeth, "Exposure fusion," in *Computer Graphics and Applications, 2007. PG '07. 15th Pacific Conference on*, Oct 2007, pp. 382–390. 2
- [21] —, "Exposure fusion: A simple and practical alternative to high dynamic range photography," *Computer Graphics Forum*, vol. 28, no. 1, pp. 161–171, 2009. [Online]. Available: <http://dx.doi.org/10.1111/j.1467-8659.2008.01171.x> 2
- [22] G. Lavoué and R. Mantiuk, "Quality Assessment in Computer Graphics," in *Visual Signal Quality Assessment*. Cham: Springer International Publishing, 2015, pp. 243–286. [Online]. Available: http://link.springer.com/10.1007/978-3-319-10368-6_{}_9 2, 3
- [23] Z. Wang and A. C. Bovik, *Modern Image Quality Assessment*. Morgan & Claypool, jan 2006, vol. 2, no. 1. 2
- [24] W. Lin and C. C. Jay Kuo, "Perceptual visual quality metrics: A survey," *Journal of Visual Communication and Image Representation*, vol. 22, no. 4, pp. 297–312, may 2011. [Online]. Available: <http://linkinghub.elsevier.com/retrieve/pii/S1047320311000204> 2
- [25] M. Čadík, M. Wimmer, L. Neumann, and A. Artusi, "Evaluation of hdr tone mapping methods using essential perceptual attributes," *Computers & Graphics*, vol. 32, no. 3, pp. 330 – 349, 2008. [Online]. Available: <http://www.sciencedirect.com/science/article/pii/S0097849308000460> 3, 9
- [26] Z. Farbman, R. Fattal, D. Lischinski, and R. Szeliski, "Edge-preserving decompositions for multi-scale tone and detail manipulation," in *ACM Transactions on Graphics (TOG)*, vol. 27, no. 3. ACM, 2008, p. 67. 3, 5, 9
- [27] R. Fattal, M. Agrawala, and S. Rusinkiewicz, "Multiscale shape and detail enhancement from multi-light image collections," *ACM Transactions on Graphics*, vol. 26, no. 3, p. 51, jul 2007. 3
- [28] J. Chen, S. Paris, and F. Durand, "Real-time edge-aware image processing with the bilateral grid," *ACM Transactions on Graphics (TOG)*, vol. 26, no. 3, p. 103, 2007. 3, 4, 9
- [29] K. He, J. Sun, and X. Tang, "Guided image filtering," in *Computer Vision – ECCV 2010*, K. Daniilidis, P. Maragos, and N. Paragios, Eds. Berlin, Heidelberg: Springer Berlin Heidelberg, 2010, pp. 1–14. 3, 4, 9
- [30] C. Tomasi and R. Manduchi, "Bilateral filtering for gray and color images," in *Computer Vision, 1998. Sixth International Conference on*. IEEE, 1998, pp. 839–846. 3, 4

- [31] E. S. Gastal and M. M. Oliveira, "Domain transform for edge-aware image and video processing," in *ACM Transactions on Graphics (TOG)*, vol. 30, no. 4. ACM, 2011, p. 69. [3, 4, 9](#)
- [32] J. Lu, K. Shi, D. Min, L. Lin, and M. N. Do, "Cross-based local multi-point filtering," *Proceedings of the IEEE Computer Society Conference on Computer Vision and Pattern Recognition*, pp. 430–437, 2012. [3](#)
- [33] M. Trentacoste, R. Mantiuk, W. Heidrich, and F. Dufrot, "Unsharp masking, countershading and halos: Enhancements or artifacts?" *Computer Graphics Forum*, vol. 31, no. 2, pp. 555–564, 2012. [3, 9](#)
- [34] Y. Li, L. Sharan, and E. H. Adelson, "Compressing and companding high dynamic range images with subband architectures," *ACM Transactions on Graphics*, vol. 24, no. 3, p. 836, jul 2005. [Online]. Available: <http://portal.acm.org/citation.cfm?doid=1073204.1073271> [3](#)
- [35] I.-S. Jang, W.-J. Kyung, T.-H. Lee, and Y.-H. Ha, "Local contrast enhancement based on adaptive multiscale retinex using intensity distribution of input image," *Journal of Imaging Science and Technology*, vol. 55, no. 4, pp. 40502–1, 2011. [3](#)
- [36] G. Eilertsen, J. Unger, and R. K. Mantiuk, "Evaluation of tone mapping operators for hdr video," in *High Dynamic Range Video*. Elsevier, 2016, pp. 185–207. [3](#)
- [37] G. Eilertsen, J. Unger, R. Wanat, and R. Mantiuk, "Perceptually based parameter adjustments for video processing operations," in *ACM SIGGRAPH 2014 Talks*, ser. SIGGRAPH '14. New York, NY, USA: ACM, 2014, pp. 74:1–74:1. [Online]. Available: <http://doi.acm.org/10.1145/2614106.2614171> [4](#)
- [38] L. Yaroslavsky, *Digital picture processing: an introduction*. Springer Science & Business Media, 2012, vol. 9. [4](#)
- [39] J.-S. Lee, "Digital image smoothing and the sigma filter," *Computer vision, graphics, and image processing*, vol. 24, no. 2, pp. 255–269, 1983. [4](#)
- [40] S. M. Smith and J. M. Brady, "Susan—a new approach to low level image processing," *International journal of computer vision*, vol. 23, no. 1, pp. 45–78, 1997. [4](#)
- [41] S. Paris, P. Kornprobst, J. Tumblin, and F. Durand, *Bilateral filtering: Theory and applications*. Now Publishers Inc, 2009. [4, 6](#)
- [42] S. Paris and F. Durand, "A fast approximation of the bilateral filter using a signal processing approach," in *European conference on computer vision*. Springer, 2006, pp. 568–580. [4](#)
- [43] S. Paris, S. W. Hasinoff, and J. Kautz, "Local laplacian filters: edge-aware image processing with a laplacian pyramid," *Communications of the ACM*, vol. 58, no. 3, pp. 81–91, 2015. [5](#)
- [44] F. Durand and J. Dorsey, "Fast bilateral filtering for the display of high-dynamic-range images," *ACM Trans. Graph.*, vol. 21, pp. 257–266, Jul. 2002. [Online]. Available: <http://doi.acm.org/10.1145/566654.566574> [5](#)
- [45] P. Burt and E. Adelson, "The laplacian pyramid as a compact image code," *IEEE Transactions on communications*, vol. 31, no. 4, pp. 532–540, 1983. [5](#)
- [46] A. Chambolle and T. Pock, "A first-order primal-dual algorithm for convex problems with applications to imaging," *Journal of mathematical imaging and vision*, vol. 40, no. 1, pp. 120–145, 2011. [5](#)
- [47] V. L. Guen, "Cartoon+ Texture Image Decomposition by the TV-L1 Model," *Image Processing On Line*, vol. 4, pp. 204–219, 2014. [Online]. Available: <http://www.ipol.im/pub/art/2014/103/> [5, 9](#)
- [48] Y. Meyer, *Oscillating patterns in image processing and nonlinear evolution equations: the fifteenth Dean Jacqueline B. Lewis memorial lectures*. American Mathematical Soc., 2001, vol. 22. [5](#)
- [49] L. Xu, C. Lu, Y. Xu, and J. Jia, "Image smoothing via l0 gradient minimization," in *ACM Transactions on Graphics (TOG)*, vol. 30, no. 6. ACM, 2011, p. 174. [5, 9](#)
- [50] A. Buades, B. Coll, and J. M. Morel, "The staircasing effect in neighborhood filters and its solution," *IEEE Transactions on Image Processing*, vol. 15, no. 6, pp. 1499–1505, 2006. [6, 8](#)
- [51] L. I. Rudin, S. Osher, and E. Fatemi, "Nonlinear total variation based noise removal algorithms," *Physica D: Nonlinear Phenomena*, vol. 60, no. 1, pp. 259 – 268, 1992. [Online]. Available: <http://www.sciencedirect.com/science/article/pii/016727899290242F> [7](#)
- [52] T. F. Chan and J. Shen, *Image processing and analysis: variational, PDE, wavelet, and stochastic methods*. SIAM, 2005. [7](#)
- [53] K. He, J. Sun, and X. Tang, "Guided image filtering," *IEEE Transactions on Pattern Analysis and Machine Intelligence*, vol. 35, no. 6, pp. 1397–1409, 06 2013. [Online]. Available: doi.ieeecomputersociety.org/10.1109/TPAMI.2012.213 [9](#)
- [54] S. Paris and F. Durand, "A fast approximation of the bilateral filter using a signal processing approach," *International journal of computer vision*, vol. 81, no. 1, pp. 24–52, 2009. [9](#)
- [55] M. Aubry, S. Paris, S. W. Hasinoff, J. Kautz, and F. Durand, "Fast local laplacian filters: Theory and applications," *ACM Trans. Graph.*, vol. 33, no. 5, pp. 167:1–167:14, Sep. 2014. [Online]. Available: <http://doi.acm.org/10.1145/2629645> [9](#)

Charles Hessel received the B.Sc. and M.Sc. degrees in electronic, electrotechnic and automation from University Toulouse III Paul Sabatier, Toulouse, France, in 2012 and 2014 respectively. He obtained a CIFRE scholarship from the French Ministry of Higher Education, Research and Innovation, and was a Ph.D. student at DxO, Boulogne-Billancourt, France, and the Centre de Mathématiques et leurs Application (CMLA), at the École Normale Supérieure Paris-Saclay, Cachan, France, from which he received the Ph.D. degree in applied mathematics in 2018. He is currently a postdoctoral researcher at the École Normale Supérieure Paris-Saclay.

Jean-Michel Morel received the PhD degree in applied mathematics from University Pierre et Marie Curie, Paris, France in 1980. He started his career in 1979 as assistant professor in Marseille Luminy, then moved in 1984 to University Paris-Dauphine where he was promoted professor in 1992. He is Professor of Applied Mathematics at the École Normale Supérieure Paris-Saclay since 1997. His research is focused on the mathematical analysis of image processing. He is a 2013 laureate of the *Grand Prix Inria-Académie des Sciences*, a 2015 laureate of the Longuet-Higgins prize, and of the 2015 CNRS *médaille de l'innovation*.